Optical and acoustic plasmons in two-layered quantum wires

V. Shikin,* T. Demel, and D. Heitmann
Max-Planck-Institut für Festkörperforschung, Heisenbergstrasse 1, D-7000 Stuttgart 80, Federal Republic of Germany
(Received 2 December 1991)

We present a theory of plasma oscillations in a two-layered quantum-wire structure. We find essentially two modes which correspond to in-phase and antiphase charge-density oscillations in the two wires and resemble optical and acoustic plasmon modes in multilayered two-dimensional electron systems.

I. INTRODUCTION

With modern lithographic techniques it has become possible to prepare very accurately defined microstructured semiconductor systems. Recently, starting from modulation-doped double-layered quantum wells in $Al_xGa_{1-x}As$-GaAs, arrays of periodic two-layered quantum wires have been prepared by deep-mesa-etching techniques.[1,2] The far-infrared excitation spectrum[2] exhibited two pronounced modes which were explained in analogy to multilayered two-dimensional electronic systems[3-5] (2DES's) as localized optical and acoustic plasmon modes.

There are already a number of publications on plasmon excitation in one-layered quantum-wire systems;[6-13] for recent reviews, see, e.g., Refs. 14–17. Here we will give, in a first step, a calculation of the plasmon modes in single one-layered quantum wires and single two-layered quantum wires. We will then extend these results to periodic arrays of wires. Since the actual equilibrium charge density in the quantum wires is not accurately known, we will present calculations for two limiting cases, (i) for a constant equilibrium charge density $n(x)=n_s$, and (ii) for an equilibrium charge density $n(x)$ that corresponds to the self-consistent distribution in an external potential of parabolic shape.

We assume that the original confinement in the growth direction (the z direction) is very strong. Thus $n(x)$ represents a two-dimensional charge density. y and x denote, respectively, the directions along and perpendicular to the wires in the plane of the original quantum well. A sketch of single- and double-layered structures is presented in Fig. 1. In the actual experimental structures in Refs. 1 and 2 the spacing d between the two layers is about 130 nm, the period is $a=1100$ nm, and the nominal geometrical width of the etched wire is $t=550$ nm. The actual width w of the electron channel is smaller due to lateral depletion. We treat w here as a free parameter and estimate it from the experimental data.

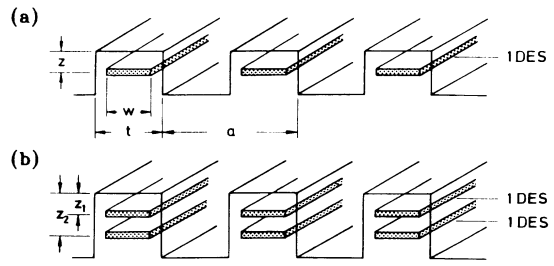

FIG. 1. Schematical configuration of one-dimensional electron systems (1DES's) in single- (a) and double-layered (b) quantum wires prepared by deep-mesa etching. Trenches are etched into an $Al_xGa_{1-x}As$-GaAs heterostructure. The periodicity is a, the geometrical width of etched wires it t, the actual lateral extent of the 1DES is w, which is smaller than t due to lateral depletion. The distance between the 1DES and the surface is z_1 for the one-layered wires and z_1 and z_2 for the two-layered case. The distance between the two layers is $z_2-z_1=d$.

Two-layered quantum-wire systems have also been considered by Katayama[18] with emphasis on the calculation of the absolute transmission strengths. In our paper we concentrate on a microscopic model to calculate the resonance frequencies from microscopic, experimentally known quantities and compare them with the experimental results.

II. THE BASIC EQUATIONS

The final aim of our calculations is to determine the spectrum of the lowest eigenmodes for a periodic array of double-layered quantum wires. However, the general results are quite complicated, so it is more effective to explain the technical details first by considering a one-layered single wire. We then expand these results to a two-layered system and then to a periodic array of wires.

A. One single quantum wire

We consider a wire with a uniform equilibrium electron density $n(x)$ inside the electron channel with edges at $\pm w/2$:

$$n(x)=\begin{cases} n_s, & -w/2\le x\le +w/2 \\ 0, & |x|>\dfrac{w}{2}\ , \end{cases} \tag{1}$$

$$-m^*\dot{v}=e\varphi'(x,t)\ , \tag{2}$$

$$\dot{\delta n}+n_s v'(x,t)=0\ , \tag{3}$$

$$\varphi'(x,t)=2\frac{e}{\kappa}\int_{-w/2}^{+w/2}\frac{\delta n(s,t)}{x-s}ds\ , \tag{4}$$

$$\int_{-w/2}^{+w/2}\delta n(s,t)ds=0 \quad \text{or} \quad v(x,t)|_{x=\pm w/2}=0\ , \tag{5}$$

$$\delta n \ll n_s\ . \tag{6}$$

Here Eq. (2) is the equation of motion, $v(x,t)$ is the velocity of the electrons, Eq. (3) is the continuity equation in the linear approximation, δn is the perturbation of the equilibrium electron density, $\delta n(x,t) \ll n_s$, Eq. (4) is the Poisson equation, $\varphi(x,t)$ is the electropotential, and m^* is the effective mass. We assume, for a moment, that the wire is embedded in a material with a uniform dielectric constant κ.

Using the new variables

$$\tilde{x}=\frac{2x}{w}, \quad \omega_\lambda^2=\frac{4e^2 n_s}{m^* w \lambda} \tag{7}$$

and evident manipulations, it is possible to reduce the system (2)–(5) to the solution of the eigenproblem

$$\varphi'(\tilde{x})=\lambda \int_{-1}^{+1} \frac{\varphi''(s)}{\tilde{x}-s} ds \ , \quad \varphi'|_{\pm 1}=0 \tag{8}$$

or

$$\varphi(\tilde{x})=\lambda \int_{-1}^{+1} \frac{\varphi'(s)}{\tilde{x}-s} ds \ , \quad \varphi'|_{\pm 1}=0 \ . \tag{9}$$

Here λ is the eigenvalue of Eq. (9). If the equilibrium density $n(x)$ is not constant we have

$$\varphi(x)+\frac{2e^2}{\omega^2 \kappa m^*} \int_{-w/2}^{+w/2} n(s) \frac{d\varphi}{ds} \frac{1}{x-s} ds \tag{10}$$

instead of Eq. (9). Equation (10) can be solved analytically at least in two limit cases:

$$\text{(i)} \quad n(x)=n_s, \quad \pm w/2 \to \pm \infty \ , \tag{11}$$

$$\text{(ii)} \quad n(x)=n_0(1-4x^2/w^2)^{1/2} \ , \quad n_0=\frac{Kw\kappa}{4\pi e^2} \ . \tag{12}$$

The charge-density distribution (i) corresponds to an infinite 2DES and (ii) corresponds to the self-consistent solution of the equilibrium problem if we assume that the external confining potential $V(x)$ in the quantum wire has a parabolic shape:

$$V(x)=V_0+\tfrac{1}{2}Kx^2 \ .$$

Here K is the curvature of the parabolic potential.

In the first case (i) we can use a Fourier transform for the solution of the equation

$$\varphi(x)=\frac{2e^2 m_s}{\omega_p^2 k m^*} \int_{-\infty}^{+\infty} \frac{d\varphi}{ds} \frac{1}{x-s} ds \ . \tag{13}$$

If

$$\varphi(x)=\varphi_0 \sin(qx), \quad \int_{-\infty}^{+\infty} \frac{\cos(q\xi)}{\xi} d\xi=0 \ , \quad \int_{-\infty}^{+\infty} \frac{\sin(q\xi)}{\xi} d\xi=\pi \ , \tag{14}$$

Eq. (13) is reduced to the well-known dispersion law[16,17]

$$\omega_p^2(q)=\frac{2\pi e^2 n_s}{\kappa m^*} q \ , \tag{15}$$

with a continuous eigenvalue spectrum corresponding to the continuous values of the plasmon wave vector q.

In the case (ii) of an electron channel with a parabolic confinement, we find for the dipole mode ω_d the solution of Eq. (10):

$$\varphi(x)=\varphi_0 x, \quad -w/2 \le x \le +w/2 \ . \tag{16}$$

Using this expression for $\varphi(x)$, the determination (12) for $n(x)$ and the integral

$$\int_{-1}^{+1} (1-\xi^2)^{1/2} \frac{d\xi}{s-\xi}=\pi s \ , \tag{17}$$

we find from Eq. (10) the dispersion law

$$\omega_d^2=K/m^* \ , \tag{18}$$

which is the same as in Ref. 19.

This result means that the dipole plasmon frequency in a quantum wire with parabolic external potential is only determined by the curvature of this external potential and, in contrast to, e.g., the "sharp" potential [Eq. (11)], is independent of the density of the electrons in the channel. This unique behavior has also been found from quantum-mechanical calculations of quantum wells and dots with a parabolic external potential[20–22] and is called the "generalized Kohn theorem."

B. The single double-layered stripe

In analogy to Sec. II A we now have for a double-layered stripe system the equations

$$i\omega \delta n_1 + n_s \, dv_1/dx=0 \ , \tag{19}$$

$$i\omega \delta n_2 + n \, dv_2/dx=0 \ , \tag{20}$$

$$v_1|_{\pm w/2}=0, \quad v_2|_{\pm w/2}=0 \ , \tag{21}$$

$$-i\omega v_1=\frac{e}{m^*}\varphi_1^* \left[x, z=\frac{d}{2}\right]+\frac{e}{m^*}\varphi_2' \left[x, z=\frac{d}{2}\right] \ , \tag{22}$$

$$-i\omega v_2=\frac{e}{m^*}\varphi_1' \left[x, z=-\frac{d}{2}\right]+\frac{e}{m^*}\varphi_2' \left[x, z=-\frac{d}{2}\right] \ , \tag{23}$$

$$\varphi_1(x,z)=\frac{2e}{\kappa} \int_{-w/2}^{+w/2} \delta n_1(s) \times \ln \frac{L}{\{(x-s)^2+[z-(d/2)]^2\}^{1/2}} ds \ , \tag{24}$$

$$\varphi_2(x,z)=\frac{2e}{\kappa} \int_{-w/2}^{+w/2} \delta n_2(s) \times \ln \frac{L}{\{(x-s)^2+[z+(d/2)]^2\}^{1/2}} ds \ . \tag{25}$$

Here L is the length of the electron channel in the y direction.

In general, this system of equations can only be solved numerically. In the following we would like to give two special representations that correspond to the energetically lowest modes of the system and are the only modes observed in the experiments in Refs. 1 and 2. In this case the numerical evaluation is easier, and, within additional approximations, it is possible to give analytical results

that elucidate the physics behind the mathematical formulation. All eigenfrequencies ω_λ and effective dielectric constants $\kappa_\pm$ given in the following correspond to these lowest modes.

The system (19)–(25) has two special representations in which the total number of variables can be reduced. First let us assume that it is possible to define

$$\delta n_+(x)=\delta n_1(x)+\delta n_2(x), \quad v_+(x)=v_1(x)+v_2(x) . \tag{26}$$

In this case we have, instead of Eqs. (19)–(25),

$$i\omega\delta n_+ + n_s\, dv_+/dx = 0 , \tag{27}$$

$$i\omega v_+(x)=\frac{2e}{\kappa}\int_{-w/2}^{+w/2}\delta n_+(s)M_+(x-s)ds , \tag{28}$$

$$M_+(x)=\frac{1}{x}+\frac{x}{x^2+d^2} , \tag{29}$$

$$v_+(x)|_{\pm w/2}=0 . \tag{30}$$

The system (27)–(30) is similar to the system (2)–(5), so it can be reduced to one equation as for Eq. (8):

$$\omega_+^2=\frac{4n_s e^2}{\kappa m^* w\lambda_+}, \quad v_+(\tilde{x})=\lambda_+\int_{-1}^{+1}M_+(\tilde{x}-s)\frac{dv_+}{ds}ds , \quad v_+(\tilde{x})|_{\pm 1}=0 . \tag{31}$$

The same possibility exists for the variables

$$\delta n_- =\delta n_1-\delta n_2, \quad v_- =v_1-v_2 . \tag{32}$$

In this case we have

$$\omega_-^2=\frac{4n_s e^2}{\kappa m^* w\lambda_-} , \tag{33}$$

$$v_-(\tilde{x})=\lambda_-\int_{-1}^{+1}M_-(\tilde{x}-s)v'_-(s)ds , \tag{34}$$

$$M_-(\tilde{x})=\frac{1}{x}-\frac{\tilde{x}}{\tilde{x}^2+4\tilde{d}^2} , \tag{35}$$

$$\tilde{d}=d/w, \quad v_-|_{\pm 1}=0 . \tag{36}$$

The physical reasons for the two types of excitations are evident. For the first mode, the electron motion in neighboring stripes is parallel (in phase); and in the second case, it is antiparallel (out of phase). These types of localized plasma oscillations resemble freely propagating "optical" and "acoustic" plasmons in multilayered 2DES's.[3–5]

If the parameter d/w is small compared to 1, Eqs. (31) and (34) can be simplified. Equation (31) in this limit is similar to (9), with n_s in Eq. (7) replaced by $2n_s$. The simplification of Eq. (34) is more essential. In this limit we have

$$\int_{-1}^{+1}M_-(\tilde{x}-s)v'_-(s)ds \simeq -v''_-(\tilde{x})\times 2\pi\tilde{d} . \tag{37}$$

In the limiting case $d/w \ll 1$, Eq. (34) can be written as

$$v''_- +\frac{\omega^2\kappa m^*}{2\pi e^2 n_s d}v_- =0, \quad v_-|_{\pm w/2}=0 . \tag{38}$$

The solution of this equation for the lowest mode is

$$\omega_-^2=\frac{2\pi^3 e^2 n_s d}{\kappa m^* w^2} . \tag{39}$$

One remark is important for the interpretation of the experiments.[1,2] So far we have assumed that the two wires are embedded in a homogeneous material with a uniform dielectric constant κ. The real experimental structures in Refs. 1 and 2 are more complex and consist of trenches with a dielectric constant $\kappa_1=1$ etched into the GaAs with the dielectric constant $\kappa_2=12.8$. Then we have the situation that for the parallel mode ω_+ the electric field is distributed mainly outside the double-layered structure, and the real distribution of the dielectric material surrounding the stripe becomes important. In principle, this fact can be taken into account in the calculations. However, it is a very complex task for the actual deep-mesa-etched structure. So we introduce an effective dielectric function κ_+, treat it as an additional free parameter, and extract this parameter from the experimental data. To be accurate we also have to introduce an effective dielectric constant κ_- for the antiparallel mode ω_-. However, in this case the electric field is localized mainly between the electron channels. So the dielectric constant κ_- in the determination of ω_-, Eq. (39), is very close to the dielectric constant of GaAs, i.e., $\kappa_-\approx\kappa_2$. Since we know ω_+ and ω_- from the experiment, we can determine κ_+ from the relation

$$\frac{\omega_+^2}{\omega_-^2}=\frac{\kappa_-\lambda_-}{\kappa_+\lambda_+}, \quad \kappa_-\approx\kappa_2\approx\kappa . \tag{40}$$

Using the determination ω_- (39) and the experimental values from Refs. 1 and 2, $\omega_-\simeq 4$ meV, $\kappa=\kappa_2=12.8$, $d=133$ nm, $m^*=0.067m_e$, we can estimate the width w of the electron channel, which gives

$$w\approx 420 \text{ nm} . \tag{41}$$

From this we deduce that the ratio $d/w\approx 0.27$ is not really a small value. So numerical calculations are necessary to give a more accurate estimate of w (approximately 20–30 %).

C. The periodical system of single-layered stripes

The original equations of plasma oscillations for a periodical system of electron stripes are quite complicated. For example, the equation of motion in the case of a periodical system of single stripes [see Fig. 1(a)] has the following structure:

$$-i\omega m^*\varphi_l=e\varphi'_l+e\varphi'_{l+1}+e\varphi'_{l-1}+\cdots , \tag{42}$$

$$\varphi'_{l+1}(x)=\frac{2e}{\kappa}\int_{-(w/2)+a}^{+(w/2)+a}\frac{\delta n_{l+1}(s)}{x-s}ds , \tag{43}$$

$$\varphi'_{l-1}(x)=\frac{2e}{k}\int_{-(w/2)-a}^{+(w/2)-a}\frac{\delta n_{l-1}(s)}{x-s}ds . \tag{44}$$

Now we can use the special property of the lowest modes $\omega_\pm$. We are interested in the solution that has no dispersion along the x direction. In particular, this means that

$$\delta n_{l+1}(\xi+a)=\delta n_l(\xi), \quad \delta n_{l-1}(\xi-a)=\delta n_l(\xi) . \tag{45}$$

Using Eqs. (45) we can transform the determinations (43), φ'_{l+1}, and (44), φ'_{l-1}:

$$\varphi'_{l+1}(x)=\frac{2e}{k}\int_{-w/2}^{+w/2}\frac{\delta n_l(\xi)}{x-\xi-a}d\xi\ , \tag{46}$$

$$\varphi'_{l-1}(x)=\frac{2e}{\kappa}\int_{-w/2}^{+w/2}\frac{\delta n_l(\xi)}{x-\xi+a}d\xi\ . \tag{47}$$

As a result, the eigenproblem for the periodic system of single stripes can be formulated as a single-stripe eigenproblem with a special type of integral kernel:

$$v_l(\tilde{x})=\lambda\int_{-1}^{+1}P(\tilde{x}-s)v'_l(s)ds\ ,\quad \omega_\lambda^2=\frac{4e^2n_s}{\kappa m^* w\lambda}\ , \tag{48}$$

$$P(\tilde{x})=\frac{1}{\tilde{x}}+\frac{1}{\tilde{x}-a/w}+\frac{1}{\tilde{x}+a/w},\quad v_l|_{\pm1}=0\ , \tag{49}$$

where ω_λ includes the renormalization of the eigenfrequency in Eq. (7) due to the interaction with the neighboring stripes.

For the calculations below it is convenient to transform Eq. (48):

$$\int_0^{\tilde{x}}v_l(s)ds=\lambda\int_{-1}^{+1}ds\ v'_l(s)\int_0^{\tilde{x}}P(s'-s)ds'\ , \tag{50}$$

or

$$\int_0^{\tilde{x}}v_l(s)ds=\lambda\int_{-1}^{+1}ds\ v_l(s)P(\tilde{x}-s)\ . \tag{51}$$

This equation has the same structure (including boundary conditions) as, e.g., Eq. (9), because, if $\int_0^{\tilde{x}}v_l ds=y$, it is

$$y(\tilde{x})=\lambda\int_{-1}^{+1}P(\tilde{x}-s)y'(ds),\quad y'|_{\pm1}=0\ . \tag{52}$$

D. The periodical system of double-layered stripes

The final eigenplasma-mode equations in the case of a periodic array of double-layered stripes can be formulated in analogy with Secs. II A and II B. The period a, the width of the electron channel w, and the distance between the wires d are defined in Fig. 1(b):

$$y(\tilde{x})=\lambda_\pm\int_{-1}^{+1}y'(s)Q_\pm(\tilde{x}-s)ds,\quad y'|_{\pm1}=0\ , \tag{53}$$

$$\begin{aligned}Q_\pm(\tilde{x})=&\frac{1}{\tilde{x}}\pm\frac{\tilde{x}}{\tilde{x}^2+4(d^2/w^2)}+\frac{2\tilde{x}}{\tilde{x}^2-4(a^2/w^2)}\\&\pm\frac{\tilde{x}-2(a/w)}{[\tilde{x}-2(a/w)]^2+4(d^2/w^2)}\\&\pm\frac{\tilde{x}+2(a/w)}{[\tilde{x}+2(a/w)]^2+4(d^2/w^2)}\ ,\\ \omega_\pm^2=&\frac{4e^2n_s}{\kappa_\pm m^* w\lambda_\pm}\ .\end{aligned} \tag{54}$$

As above, the modes ω_+ and ω_- have different effective dielectric constants, κ_+ and κ_-, respectively. The generalization of Eq. (53) for an arbitrary equilibrium distribution $n(x)$ corresponds to the transition from Eq. (9) to Eq. (10).

III. NUMERICAL CALCULATIONS AND DISCUSSIONS

For a solution of Eqs. (9), (10), (31), (34), (52), and (53), it is convenient to use the system of Tschebyscheff polynomials: $T_m(x)$ and $U_m(x)$.[23] We can assume that, e.g., in the case of Eq. (9),

$$\begin{aligned}\varphi'(x)=(1-x^2)^{1/2}[&v_0U_0(x)+v_2U_2(x)\\&+v_{2i}U_{2i}(x)+\cdots]\ .\end{aligned} \tag{55}$$

This determination of $\varphi'(x)$ satisfies the boundary condition in Eqs. (5) and (9) and has arbitrary coefficients v_{2i}, $i=0,1,2\ldots$. Using the presentation (55) for φ' and the corresponding properties of the polynomials $T_m(x)$ and $U_m(x)$, it is not difficult to reduce Eqs. (9), (10), (31), (34), (52), and (53) for a numerical solution of the matrix problem with respect to the coefficient v_{2i}. The convergency of the presentation (55) is good. The eigen-numbers calculated with a 6×6 matrix are within 1% accuracy identical to calculations with an 8×8 matrix. The most interesting results of these calculations for the periodical system of double-layered stripes are presented in Fig. 2. They correspond to the solution of Eq. (53) with a uniform distribution of the dielectric constant κ and a constant equilibrium charge-density distribution in the wire, $n(x)=n_s$. The calculations show that the frequencies of the lowest modes do not strongly depend on the shape of the confining potential and the electron distribution $n(x)$. To give some examples: The ratio between the ω_+ and the ω_- modes for $d/w=0.25$ (0.5, 0.75, 1.0) is $\omega_+/\omega_-=2.54$ (1.60, 1.30, 1.18) for a model with $n(x)=n_s=$const. For the model with $n(x)\propto(1-4x^2/w^2)^{1/2}$ we calculate $\omega_+/\omega_-=2.60$ (1.61, 1.30, 1.18).

For the normalization of $\omega_\pm^2$ in Fig. 2 we use the fre-

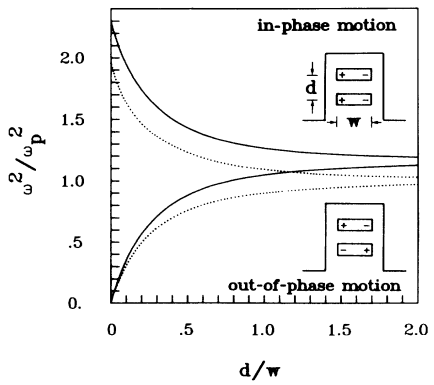

FIG. 2. The calculated normalized plasmon frequencies $\omega_\pm/\omega_p$ vs d/w with a fixed parameter a/w and for a constant charge distribution $n(x)=n_s$ in the channel. The solid lines correspond to $a/w=100$, the dashed lines correspond to $a/w=2$. The frequency ω_p for the normalization is $\omega_p^2=4\pi e^2n_s/\kappa m^* w$. The insets show schematically the charge distribution for the in-phase, "optical" plasma oscillation (top, ω_+) and for the out-of-phase, "acoustic" plasma oscillation (bottom, ω_-).

quency ω_p:

$$\omega_p^2 = \frac{4\pi e^2 n_s}{\kappa m^* w} .$$

This choice is convenient for a comparison with the corresponding numerical calculations of ω by Eliasson *et al.*[12] Our results for ω/ω_p in Fig. 2 in the limit $a/w \gg 1$, $d/w \gg 1$ coincide with the calculations in Ref. 12 (see Fig. 1 there).

As indicated above, due to the assumption of a uniform κ, the presented theory can be directly used for the interpretation of the soft mode ω_- only. With the experimental values from Refs. 1 and 2, i.e., $a = 1100$ nm, $d = 133$ nm, $n_s = 4.2 \times 10^{11}$ cm^{-2} (from SdH measurements), $\kappa_2 = 12.8$, $m^* = 0.067 m_e$, and the experimental resonance frequency of $\omega_- = 34$ cm^{-1}, we can determine from Fig. 2 the width of the electron channel in the double-layered structure and find

$$w = 448 \text{ nm} . \tag{56}$$

This result for w seems reasonable, because, due to the lateral depletion, w is smaller than the nominal geometrical width of the deep-mesa-etched structure, $t = 550$ nm. This lateral depletion length, $l_d = 0.5(t - w)$, follows to be $l_d \approx 50$ nm, which is consistent with other determinations, e.g., those in Ref. 24. It is also suitable to compare the estimations of w from Eqs. (56) and (41). The agreement between these numbers is quite good.

From the experimental value[1,2] of $\omega_+ = 64$ cm^{-1}, from the estimation (56) of w via ω_-, and from the determination (40) of κ_+ we find

$$\kappa_+ \approx 6.9 . \tag{57}$$

κ_+ should be given approximately by the average $0.5(\kappa_1 + \kappa_2)$ of the dielectric constants of vacuum, $\kappa_1 = 1$, and of GaAs, $\kappa_2 = 12.8$. Thus the result (57) is reasonable.

We would now like to comment on Ref. 18, which contains a discussion of a similar problem. The most important result of this paper is the direct demonstration of the possibility of exiting in a double-layered structure both the ω_+ mode and the ω_- mode using excitation with a uniform electric field. In particular, it describes nicely the experimentally observed asymmetry of the transmission strength for the two modes. In detail there are some open questions in the paper concerning the prediction of a universal gap Ω_0 in the general plasma dispersion law $\omega(q_x)$ in Fig. 3 of Ref. 18. In Ref. 18 the effective one-electron potential $U(x)$ in the many-electron system is characterized by a frequency Ω_0 [Eq. (B1)], which is identified with the dipole plasma frequency [Eq. (B15)]. But it is well known[6,7,19–22] (see the discussion of the generalized Kohn theorem above) that the dipole plasma frequency is governed by the frequency $\Omega_*^2 = K/m^*$ of the external potential [Eq. (18)], whereas the effective one-electron potential, which is characterized by the frequency Ω_0 and can be measured in Shubnikov–de Haas experiments,[7,8,24] is drastically reduced in the systems of interest here due to screening. Thus the real gap Ω_* should have the scale $\Omega_*^2 \propto \Omega_0^2(w/a_b)$, where a_b is the Bohr radius.[19] Since $a_b \approx 10$ nm for GaAs we have $w/a_b \gg 1$. Therefore it is important to take this renormalization of Ω_0 into account. Moreover, in our microscopic ansatz we have the possibilities of investigating the properties of $\omega_\pm$ in their dependence on the microscopic parameters, d/w, a/w, the distribution $n(x)$, and the distribution of dielectrica.

In this paper we have concentrated on the experimental situation in Ref. 1 and restricted ourselves to excitations with the electric-field vector perpendicular to the quantum wire ($q_y = 0$). It is also interesting to consider excitations with $q_y > 0$, where plasmons propagate freely along the wires. Such excitations have recently been observed in far-infrared experiments on single-layered quantum-wire arrays,[25] and in Raman experiments on multilayered quantum-wire systems.[26] One finds that each of the different plasmon branches at $(q_x, q_y = 0)$ exhibits a dispersion with increasing q_y. This is in agreement with the theoretical treatments for one-layered wire systems.[9–13] In particular, recent calculations by Li[27] for five-layered quantum-wire arrays confirm beautifully the q_x and q_y dispersion observed by Egeler *et al.*[26]

*Permanent address: Institute of Solid State Physics, 142432 Cernogolovka, U.S.S.R.

[1]T. Demel, D. Heitmann, P. Grambow, and K. Ploog, Phys. Rev. B **38**, 12 732 (1988).
[2]T. Demel, D. Heitmann, P. Grambow, and K. Ploog, Superlatt. Microstruct. **5**, 287 (1989).
[3]G. Fasol, N. Mestres, H. P. Hughes, A. Fischer, and K. Ploog, Phys. Rev. Lett. **56**, 2517 (1986).
[4]A. Pinczuk, M. G. Lamont, and A. C. Gossard, Phys. Rev. Lett. **56**, 2092 (1986).
[5]J. K. Jain and P. B. Allen, Phys. Rev. Lett. **54**, 2437 (1985).
[6]W. Hansen, M. Horst, J. P. Kotthaus, U. Merkt, Ch. Sikorski, and K. Ploog, Phys. Rev. Lett. **58**, 2586 (1987).
[7]J. Alsmeier, Ch. Sikorski, and U. Merkt, Phys. Rev. B **37**, 4314 (1988).
[8]F. Brinkop, W. Hansen, J. P. Kotthaus, and K. Ploog, Phys. Rev. B **37**, 6547 (1988).
[9]S. Das Sarma and W. Y. Lai, Phys. Rev. B **32**, 1401 (1985).
[10]W. Y. Lai, A. Kobayashi, and S. Das Sarma, Phys. Rev. B **34**, 7380 (1986).
[11]W. Que and G. Kirczenow, Phys. Rev. B **37**, 7153 (1988); **39**, 5998 (1989).
[12]G. Eliasson, Ji-Wei Wu, P. Harylak, and J. J. Quinn, Solid State Commun. **60**, 41 (1986).
[13]W. Que, Phys. Rev. B **43**, 7127 (1991).
[14]T. Demel, D. Heitmann, and P. Grambow, in *Spectroscopy of Semiconductor Microstructures*, edited by G. Fasol, A. Fasolino, and P. Lugli (Plenum, New York, 1989), p. 75.
[15]U. Merkt, Ch. Sikorsky, and J. Alsmeier, in *Spectroscopy of Semiconductor Microstructures* (Ref. 14), p. 89.
[16]D. Heitmann, Surf. Sci. **170**, 332 (1986).
[17]A. V. Chaplik, Superlatt. Microstruct. **6**, 329 (1989).

[18]S. Katayama, J. Phys. Soc. Jpn. **60**, 1123 (1991).
[19]V. Shikin, T. Demel, and D. Heitmann, Surf. Sci. **229**, 276 (1990).
[20]P. Ruden and G. H. Döhler, Phys. Rev. B **27**, 3547 (1983).
[21]L. Brey, N. Johnson, and P. Halperin, Phys. Rev. B **40**, 10 647 (1989).
[22]P. Maksym and T. Chakraborty, Phys. Rev. Lett. **65**, 108 (1990).
[23]H. Bateman, *Higher Transcendental Functions* (McGraw-Hill, New York, 1953), Vol. 2.
[24]T. Demel, D. Heitmann, P. Grambow, and K. Ploog, Appl. Phys. Lett. **53**, 2176 (1988).
[25]T. Demel, D. Heitmann, P. Grambow, and K. Ploog, Phys. Rev. Lett. **66**, 2657 (1991).
[26]T. Egeler, G. Abstreiter, G. Weimann, T. Demel, D. Heitmann, P. Grambow, and W. Schlapp, Phys. Rev. Lett. **65**, 1804 (1990).
[27]Q. P. Li, Solid State Commun. **80**, 767 (1991).

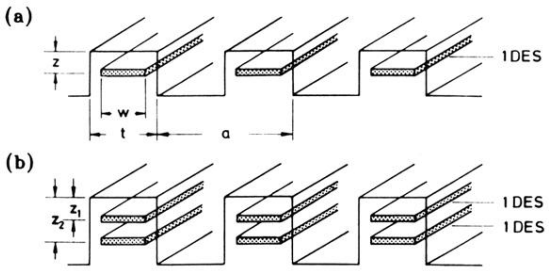

FIG. 1. Schematical configuration of one-dimensional electron systems (1DES's) in single- (a) and double-layered (b) quantum wires prepared by deep-mesa etching. Trenches are etched into an $Al_xGa_{1-x}As$-GaAs heterostructure. The periodicity is a, the geometrical width of etched wires it t, the actual lateral extent of the 1DES is w, which is smaller than t due to lateral depletion. The distance between the 1DES and the surface is z_1 for the one-layered wires and z_1 and z_2 for the two-layered case. The distance between the two layers is $z_2 - z_1 = d$.